RESEARCH ARTICLE

Metal–Support Interactions on Ag/Co$_3$O$_4$ Nanowire Monolithic Catalysts Promoting Catalytic Soot Combustion

Xingwang Yi[1,2,3] · Yuexi Yang[1,2] · Dawei Xu[1,2,3] · Ye Tian[1,2,3] · Song Song[1,2,3] · Chunmei Cao[4] · Xingang Li[1,2,3]

Abstract

Tuning metal–support interactions (MSIs) is an important strategy in heterogeneous catalysis to realize the desirable metal dispersion and redox ability of metal catalysts. Herein, we use pre-reduced Co$_3$O$_4$ nanowires (Co-NWs) in situ grown on monolithic Ni foam substrates to support Ag catalysts (Ag/Co-NW-R) for soot combustion. The macroporous structure of Ni foam with crossed Co$_3$O$_4$ nanowires remarkably increases the soot–catalyst contact efficiency. Our characterization results demonstrate that Ag species exist as Ag^0 because of the equation $Ag^+ + Co^{2+} = Ag^0 + Co^{3+}$, and the pre-reduction treatment enhances interactions between Ag and Co$_3$O$_4$. The number of active oxygen species on the Ag-loaded catalysts is approximately twice that on the supports, demonstrating the significant role of Ag sites in generating active oxygen species. Additionally, the strengthened MSI on Ag/Co-NW-R further improves this number by increasing metal dispersion and the intrinsic activity determined by the turnover frequency of these oxygen species for soot oxidation compared with the catalyst without pre-reduction of Co-NW (Ag/Co-NW). In addition to high activity, Ag/Co-NW-R exhibits high catalytic stability and water resistance. The strategy used in this work might be applicable in related catalytic systems.

Keywords Metal–support interaction · Monolithic catalysts · Ag · Co$_3$O$_4$ nanowires · Soot oxidation

Introduction

Presently, diesel engines are widely used in heavy-duty vehicles because of their low operating costs, excellent durability, superior fuel efficiency, and reliability under lean conditions [1–3]. However, soot particulates emitted from diesel engines have caused severe damage to human health and the environment [4]. Catalytic combustion technology using oxidation catalysts combined with a diesel particulate filter is a promising after-treatment strategy to trap and eliminate soot particulates in the range of 200–500 °C [5, 6].

Numerous catalysts for soot combustion have been reported using noble metals [7–9], perovskites [10, 11], spinel-type oxides [12, 13], hydrotalcites [14, 15], alkaline metal oxides [16, 17], transition metal oxides [18], and rare earth metal oxides [19]. Ag-based catalysts are promising candidates for catalytic soot oxidation reactions because of their low price among noble metals, and particularly the Ag^0 species has a high ability to activate oxygen [20–22]. Interestingly, the Ag^0 species can be automatically obtained by directly supporting Ag salt on reducible metal oxides (Co$_3$O$_4$, CeO$_2$, MnO$_2$, etc.) because of the reaction between silver and variable valence cations (for example, $Ag^+ + Co^{2+} = Ag^0 + Co^{3+}$) [7]. However, because of the increased cation valence on supports (such as $Co^{2+} \rightarrow Co^{3+}$), the number of oxygen vacancies on the surface of reducible supports will inevitably be reduced. Nevertheless, oxygen vacancies play important roles in anchoring metal sites, increasing metal dispersion, and tuning the metal–support interaction, which significantly influence the activity and stability of catalysts; moreover, they are beneficial to promoting

✉ Chunmei Cao
   caochunmei@zzu.edu.cn

✉ Xingang Li
   xingang_li@tju.edu.cn

1   School of Chemical Engineering & Technology, Tianjin University, Tianjin 300350, China

2   Institute of Shaoxing, Tianjin University, Shaoxing 312000, China

3   Collaborative Innovation Center of Chemical Science and Engineering (Tianjin), Tianjin Key Laboratory of Applied Catalysis Science and Engineering, Tianjin University, Tianjin 300350, China

4   School of Chemical Engineering, Zhengzhou University, Zhengzhou 45000, China
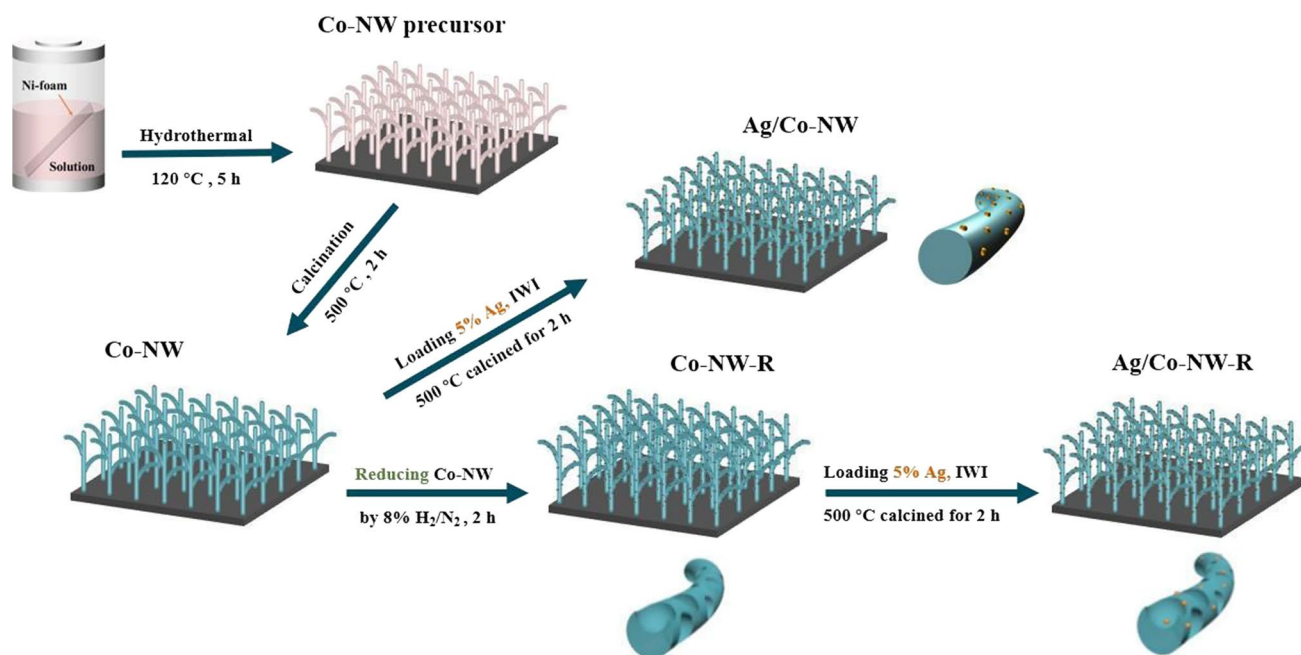
Scheme 1 Schematic diagram of the synthesis of the as-prepared catalysts on monolithic Ni foam

oxidation reactions [23–26]. Thus, before loading metals, a possible way to solve the problem is by pre-reducing reducible supports to construct more available oxygen vacancies. To date, few reports have used this strategy to develop efficient catalysts for soot combustion [27].

Some reducible, noble metal-free metal oxides, such as CeO$_2$ and MnO$_2$ and particularly Co$_3$O$_4$, are active in soot oxidation [27]. Moreover, Co$_3$O$_4$ exhibits a high ability for NO oxidation to NO$_2$ [22, 28], which is a more effective oxidant than O$_2$ for soot oxidation. Thus, Co$_3$O$_4$ becomes a good candidate for supporting noble metal catalysts in this reaction.

In addition, soot is a type of particulate with a diameter of 25–100 nm, which makes touching the inner surface of mesopores and micropores in traditional powder catalysts difficult during a reaction, resulting in low soot–catalyst contact efficiency and unsatisfactory catalytic performance [29]. To solve this problem, Zhao's research group [12, 30, 31] developed a series of three-dimensional ordered macroporous catalysts using the colloidal crystal template method for catalytic soot elimination, which can greatly improve the contact efficiency and catalytic soot oxidation performance. Zhang's group [32, 33] focused on multiple strategies to decrease the ignition temperature of soot combustion. In addition, our group [1, 5, 34] has developed a series of three-dimensional monolithic catalysts by in situ growth of nanostructured active components on monolithic substrates, which can provide a sufficient open macroporous structure to increase soot–catalyst contact opportunities and remarkably lower soot elimination temperatures.

In this work, we designed and synthesized Ag catalysts supported on pre-reduced Co$_3$O$_4$ nanowires (Co-NW) using Ni foams as the monolithic substrate for soot oxidation. The structure–activity relationship was revealed through various characterization techniques, such as scanning electron microscopy (SEM), high-resolution transmission electron microscopy (HRTEM), X-ray diffraction (XRD), X-ray photoelectron spectroscopy (XPS), temperature-programmed reduction by soot (soot-TPR), temperature-programmed oxidation by NO (NO-TPO), and CO temperature-programmed desorption (CO-TPD) measurements. The pre-reduction of the Co-NW support enhances metal–support interactions on Ag/Co-NW-R and then increases the metal dispersion and the number of oxygen vacancies and improves the turnover frequency (TOF) and catalytic performance for soot oxidation.

Experimental

Catalyst Preparation

Ag/Co$_3$O$_4$ nanowires on Ni foam were synthesized via a simple hydrothermal and incipient wetness impregnation method [1], as illustrated in Scheme 1.

The Ni foam (thickness: ca. 1.5 mm, porosity: ≥ 98%, and mechanical strength: ≥ 1 MPa) was purchased from LANKE battery materials Co. Ltd. The Ni foam was immersed in 2 mol/L HCl in an ultrasound bath for 5 min to remove the surface oxide layers and then rinsed with deionized water

and absolute ethanol for 5 min, respectively. In a typical synthesis, 1 mmol of $Co(NO_3)_2 \cdot 6H_2O$, 2 mmol of NH_4F, and 5 mmol of $CO(NH_2)_2$ were dissolved in 50 mL of water. After intense stirring for 30 min, the solution was transferred into a 100-mL Teflon-lined stainless steel autoclave. Subsequently, a piece of the clean Ni foam was immersed in the reaction solution. The autoclave was sealed and maintained at 120 °C for 5 h and cooled naturally to room temperature. The as-synthesized precursor was ultrasonically cleaned with water for 5 min and rinsed with absolute ethanol three times. After drying at 60 °C, the precursor was calcined at 500 °C in air for 2 h and denoted as Co-NW. The clean Ni foam substrate was also calcined for 2 h at 500 °C for comparison and denoted as Ni foam.

Ag/Co-NW was prepared using the impregnation method. The Co-NW precursor was impregnated with an aqueous solution of silver nitrate, followed by drying at 60 °C, and then annealed at 500 °C in air for 2 h. This catalyst was designated as Ag/Co-NW. For comparison, Co-NW was pre-reduced at 200 °C in 8% H_2/N_2 flow, and then Ag was impregnated on Co-NW-R with the same procedure of Ag/Co-NW, and the obtained catalyst was denoted as Ag/Co-NW-R. The pre-reduced Co-NW was also calcined for 2 h in 500 °C for comparison and denoted as Co-NW-R. According to the inductively coupled plasma (ICP) method (Vista MPX instrument), the loading of silver in the prepared catalysts amounted to 5 wt% (the mass fraction of Ag in the catalyst without the Ni foam substrate).

Catalyst Characterizations

The samples were characterized by XRD on a Rigaku D/MAX-2500 diffractometer (Cu Kα radiation), XPS on an ESCALAB instrument, SEM on a Hitachi S-4800 scanning electron microscope, and transmission electron microscopy (TEM) and EDS mapping on a JEOL-JEM-2100F electron microscope.

On the basis of the diameter (d) of Ag on catalysts determined by TEM, the dispersity (D_{Ag}) of Ag crystallites was calculated from the expression D_{Ag} (%) = 1.34/d, assuming that they had a spherical morphology [35].

Soot temperature-programmed reduction (soot-TPR) tests were performed in a fixed-bed reactor at a heating rate of 5 °C/min in N_2 (100 mL/min) on a CO–CO_2 IR analyzer. NO temperature-programmed oxidation (NO-TPO) experiments were measured on the same reactor with 250 mg of catalyst in 600-ppm NO/10% O_2/N_2 (100 mL/min) at a rate of 5 °C/min and recorded using a chemiluminescence $NO - NO_2 - NO_x$ analyzer (Model 42i-HL, Thermo Scientific).

H_2 temperature-programmed reduction (H_2-TPR) tests were performed on a TP-5080 instrument (50-mg sample, 8% H_2/N_2, 10 °C /min). CO temperature-programmed

desorption (CO-TPD) experiments were performed on the same instrument equipped with a mass spectrometer (Hiden). Before CO-TPD, the catalysts were pretreated at 100 °C in He flow and then adsorbed 7% CO/N_2 for 1 h. After cooling to room temperature, the system was switched to He flow and heated to 900 °C at a rate of 10 °C/min.

Catalytic Activity Measurement

The catalytic activities for soot oxidation were evaluated by soot temperature-programmed oxidation (soot-TPO) using Printex-U soot (Degussa) as a model in a fixed-bed flow reactor. To achieve the loose contact condition between catalysts and soot particulates, 15 mg of soot was dispersed in 25 mL of ethanol by ultrasound to obtain a suspended soot-ethanol solution, which was gradually dropped on the monolithic catalyst via a precisely controlled pipette gun, and then the mixture was dried at 60 °C for 2 h. The mass ratio of soot/catalyst (excluding the weight of the Ni foam substrate) was approximately 1:10. For each reaction, the monolithic catalyst was heated from 200 to 650 °C at a heating rate of 2 °C/min in the reactant gas flow (100 mL/min) of 0- or 600-ppm NO and 10% O_2 balanced with N_2. The products of CO_2 and CO were online analyzed by an IR analyzer. The catalytic activities were evaluated using the temperatures at 10% (T_{10}) and 50% (T_{50}) soot conversion during the soot-TPO reaction. The CO_2 selectivity (S_{CO_2}) was defined as $S_{CO_2} = C_{CO_2}/(C_{CO} + C_{CO_2})$, where C_{CO} and C_{CO_2} were the concentrations of CO and CO_2, respectively.

Isothermal Kinetic Measurements

The isothermal kinetic experiments (isothermal reactions and isothermal anaerobic titrations) were performed to calculate reaction rates, active oxygen amounts, and TOF values of the monolithic catalysts [36]. To ensure that all reactions occurred in the dynamic region with a low soot conversion (< 10%), the isothermal oxidation tests were conducted in a 10% O_2/N_2 flow at 280 °C (150 mL/min). When the CO_2 concentration became steady, the 10% O_2/N_2 flow was switched to a pure N_2 flow at the same volume flow rate, and the isothermal anaerobic titration began. The outlet gas was monitored online by an infrared gas analyzer. The reaction rate (ν) was calculated according to the following equation:

$$\nu = -dn/(mdt) = Q \times c/m \tag{1}$$

where Q is the molar gas flow rate (mol/s); c is the molar fraction of CO_2 estimated by isothermal reactions; and m is the mass of the catalyst (g); n is the amount of substance of CO_2 (mol).

The number of active oxygen species (O*) was quantified by integrating the diminishing rate of CO_2 concentration with time. The TOF was obtained as follows:

$$O * \text{amount(mol/g)} = 2P_0 \times V \times A \times 10^{-6}/(R \times T \times m) \tag{2}$$

$$\text{TOF} \left(s^{-1}\right) = v/O * \tag{3}$$

where P_0 represents the atmospheric pressure (Pa); V represents the volumetric flow rate (m³/s); A represents the integral of the CO_2 concentration curves as a function of time during the isothermal anaerobic titration (s); R represents the ideal gas constant; T represents the room temperature (K).

Results and Discussion

Catalyst Characterizations

Structural Properties

XRD patterns of the monolithic catalysts are shown in Fig. 1. For all as-prepared catalysts, three strong diffraction peaks are observed at $2\theta = 44.5°$, $51.8°$, and $76.2°$, which belong to metallic Ni (JPCDS 04–0850) [34]. Meanwhile, three weak peaks associated with the NiO (JPCDS 47–1049) phase are observed at $37.2°$, $43.2°$, and $62.6°$. As for Co-NW and Ag/Co-NW, the four peaks located at $31.1°$, $36.8°$, $59.2°$, and $65.1°$ can be ascribed to the (220), (311), (511), and (400) lattice planes of Co_3O_4 (JPCDS 43–1003) [7], respectively. Figure 1b shows a zoom-in of Fig. 1a, and no diffraction peak related to Ag is observed, which may result from the low loading amount and small crystallite size of Ag on the catalysts.

In Fig. 2, the structure of the as-prepared catalysts, the average diameter of silver on the Co-NW surface, and the features of Ag-Co₃O₄ composites are investigated using SEM and TEM. Figure S1 displays the SEM images of the Ni foam, which possesses a 3D-macroporous structure with diameters ranging from 200 to 500 μm. In Fig. 2a, d and g, the monolithic catalysts exhibit nanowire morphology, which is well-distributed on the skeleton of the Ni foam substrate. The nanowires are self-assembled into grass-like clusters, which can provide enough macroporous space for soot deposition [5]. The HRTEM images in Fig. 2c, f and i demonstrate that these nanowires are composites of Co_3O_4 [21].

After loading Ag, the crossed nanowire morphology of Ag/Co-NW and Ag/Co-NW-R remain unchanged, except that the surface of the nanowire becomes slightly rough in Fig. 2 a, d and g. The lattice spacing of 0.236 nm belonging to Ag (111) in Fig. 2f, i confirms the presence of metallic Ag on the catalysts [21]. In Fig. S2, Ag nanoparticles (NPs) are homogeneously dispersed on Co_3O_4 nanowires with a low content from TEM-EDS mapping. Moreover, as shown in Fig. S3j, k, the average size of Ag NPs is approximately 5.8 nm and 4.4 nm for Ag/Co-NW and Ag/Co-NW-R, respectively. We calculated the dispersion of Ag based on the above results and found that it was approximately 1.5-fold larger on Ag/Co-NW-R compared to Ag/Co-NW, as shown in Table S1.

Redox Properties

The soot-TPR and CO-TPD experiments were performed to investigate the active oxygen species of the catalysts. As shown in Fig. 3, the soot-TPR curves of the catalysts consist of three temperature ranges, representing three types of oxygen species. The low-temperature soot-TPR reduction peak at 200–400 ℃ can be assigned to interfacial active oxygen species in the case of Ag–O–Co, which is probably caused by the strong interaction between Ag and Co_3O_4. These oxygen species can be assigned to surface-adsorbed oxygen species. In addition, the peaks at 400–650 °C originate from surface lattice oxygen (O^{2-}), and the peaks above 650 °C are ascribed to the bulk lattice oxygen (O^{2-}) of the catalysts, which has little impact on the catalytic activity [5]. Compared with soot, CO is more easily oxidized, so CO-TPD

Fig. 1 XRD patterns of the as-prepared catalysts: Ni foam, Co-NW, Ag/Co-NW, and Ag/Co-NW-R. **a** Full patterns and **b** zoom-in
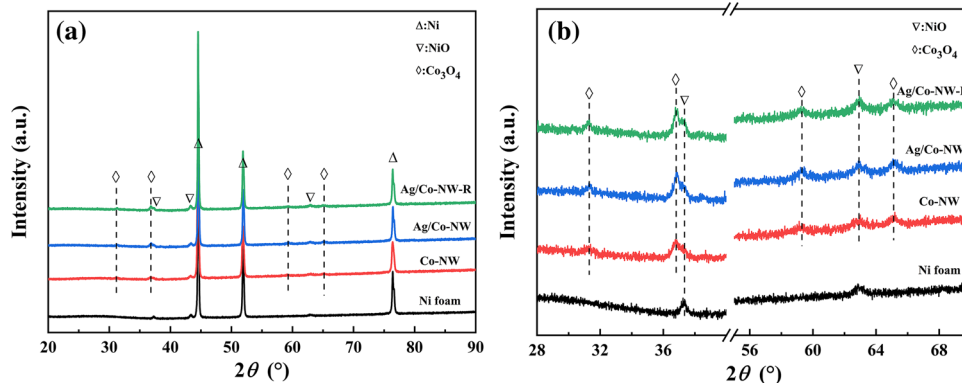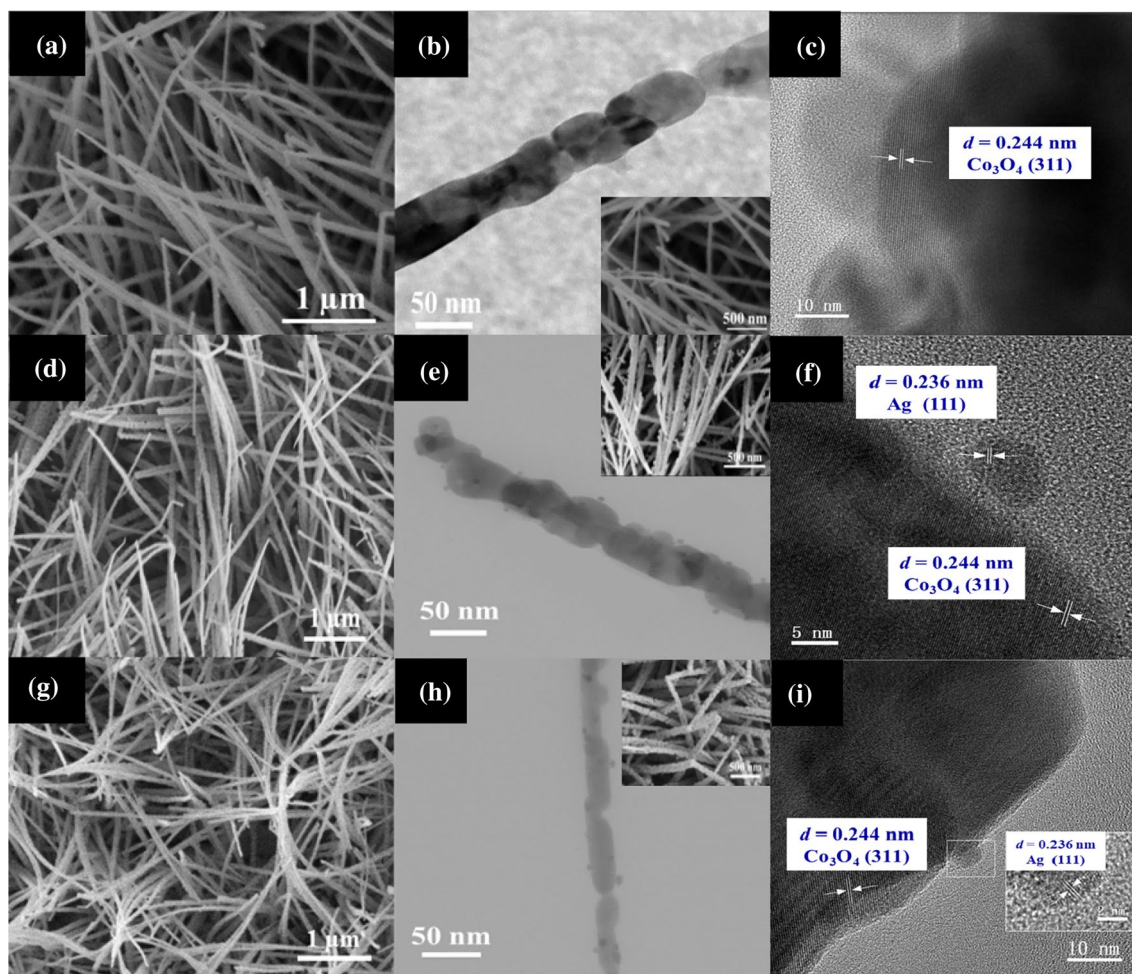
Fig. 2 Electron microscope characterization of the catalysts **a1–a3** Co-NW, **b1–b3** Ag/Co-NW, and **c1–c3** Ag/Co-NW-R; **a1–c1** SEM images, **a2–c2** TEM and SEM images, **a3–c3** HRTEM images
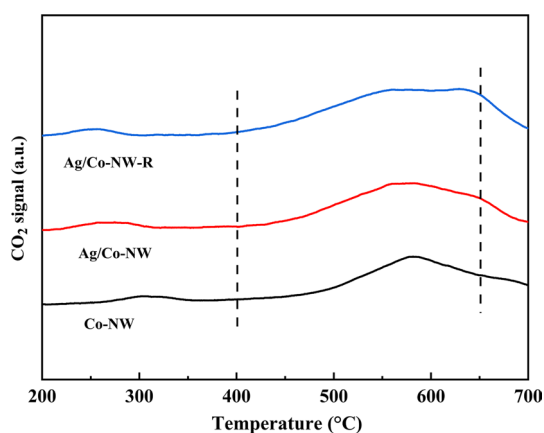

Fig. 3 Soot-TPR profiles of the catalysts

can be a better technology than soot-TPR for revealing the activity of oxygen species on the catalyst [37]. Generally, the adsorbed CO reacts with the reactive oxygen species on the catalyst and then is oxidized to CO_2 during the temperature-programmed process [37, 38]. Figure 4 shows the CO-TPD profiles of the samples. The desorption peaks below 200 °C are attributed to the desorption of CO_2 produced directly by the reaction of adsorbed CO with surface-adsorbed oxygen species. The broad peaks between 200 and 350 °C for all three catalysts belong to the desorption of CO_2 oxidized by surface lattice oxygen species. No obvious difference in the shape of the peaks is apparent for all catalysts below 350 °C. The peaks above 350 ºC can be ascribed to the desorption of CO_2 oxidized by bulk lattice oxygen species. According to the temperature range (200–600 °C) for soot oxidation, surface-adsorbed oxygen species and surface lattice oxygen species are the main active oxygen species over these catalysts [1]. For soot-TPR and CO-TPD, the peaks of surface-adsorbed oxygen species and bulk lattice oxygen species
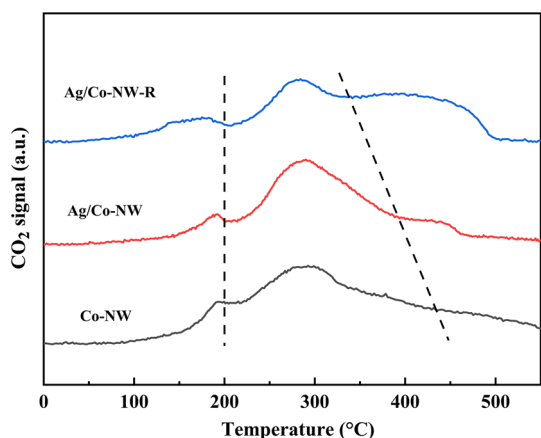
Fig. 4 CO-TPD profiles of the catalysts

for the Ag-loaded catalysts shift to lower temperatures, particularly for Ag/Co-NW-R, which illustrates that Ag-Co₃O₄ interactions can activate surface oxygen species and promote bulk lattice oxygen mobility. In Figs. 3, 4, the peak areas of the catalysts follow the order of Ag/Co-NW-R > Ag/Co-NW > Co-NW, which illustrates that Ag/Co-NW-R possesses more active oxygen species than other catalysts.

Surface Chemical States

Figure 5 and Table 1 display the XPS results of the samples. In Fig. 5a, Ag species display Ag $3d_{5/2}$ and Ag $3d_{3/2}$ peaks at binding energies of 368.0, 368.3, 374.0, and 374.3 eV, respectively, with a splitting value of 6.0 eV, which demonstrates that Ag species exist in the metallic state on the catalysts [25, 39]. Notably, the peaks of Ag/Co-NW-R shift to higher binding energy (BE) compared with Ag/Co-NW, demonstrating the enhanced metal–support interaction on Ag/Co-NW-R, which is also suggested by the decreased size of Ag NPs [27] in Fig. 2.

In Fig. 5b, the Co 2p XPS spectra of the catalysts show spin–orbit splitting into Co $2p_{1/2}$ and Co $2p_{3/2}$, which can be deconvoluted into Co^{3+}, Co^{2+}, and two weak satellite peaks at relatively high binding energies (800–810 and 786–791 eV, respectively) [1]. As listed in Table 1, Co species exist as Co^{3+} (779.5, 794.3 eV) and Co^{2+} (781.4, 795.6 eV) [40]. Additionally, the spin–orbit splitting energy between the two peaks is 15.2 eV, which indicates that the surface cobalt species exist as Co₃O₄ [41]. The values of surface $Co^{2+}/(Co^{2+}+Co^{3+})$ for all samples were calculated according to the corresponding peak areas in the XPS spectra. Notably, Co-NW-R possesses a higher Co^{2+} concentration than Co-NW, indicating that the reduction pretreatment indeed created many Co^{2+} species on Co-NW-R, as we proposed. Loading Ag on the supports consumed Co^{2+} cations according to $Ag^+ + Co^{2+} = Ag^0 + Co^{3+}$. However,
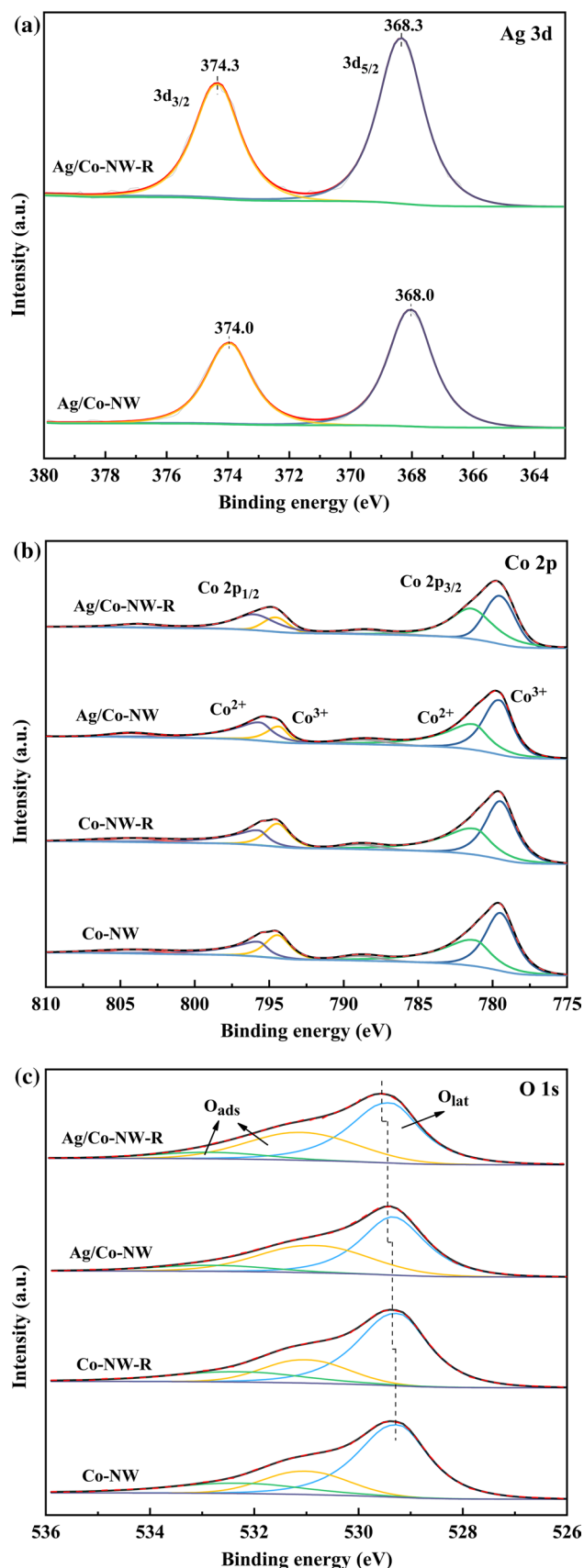

Fig. 5 XPS spectra of the catalysts: **a** Ag 3d, **b** Co 2p, and **c** O 1 s

Table 1 BE of Co 2p and O 1 s core levels and the ratio of $Co^{2+}/(Co^{2+}+Co^{3+})$ and $O_{ads}/(O_{ads}+O_{ads})$ for the as-prepared catalysts

Catalysts	Co 2p			O 1 s		
	Co^{3+} (eV)	Co^{2+} (eV)	$Co^{2+}/(Co^{3+}+Co^{2+})$	O_{ads} (eV)	O_{lat} (eV)	$O_{ads}/(O_{ads}+O_{lat})$
Co-NW	779.5, 794.3	781.4, 795.6	0.47	531.0, 532.2	529.2	0.38
Co-NW-R	779.5, 794.4	781.4, 795.7	0.49	531.1, 532.3	529.3	0.40
Ag/Co-NW	779.6, 794.4	781.5, 795.7	0.52	530.8, 532.8	529.4	0.44
Ag/Co-NW-R	779.6, 794.6	781.5, 796.1	0.56	531.1, 532.8	529.6	0.47

we interestingly observed an increased value of $Co^{2+}/(Co^{2+}+Co^{3+})$ on Ag/Co-NW and particularly on Ag/Co-NW-R. This result indicates that the enhanced Ag–Co_3O_4 interaction can generate more Co^{2+} species on the catalyst surface, which commonly accompanies the generation of oxygen vacancies to generate active oxygen species [7].

In Fig. 5c, the O 1 s XPS spectra are deconvoluted into three peaks. The peak at approximately 529.4 eV corresponds to surface lattice oxygen (O_{lat}), and the peaks at approximately 531.0 and 532.8 eV agree with oxygen species such as O_2^- and O_2^{2-} adsorbed on oxygen vacancies (O_{ads}) [42]. In Table 1, compared with Co-NW, Co-NW-R exhibits a higher ratio of $O_{ads}/(O_{ads}+O_{lat})$, demonstrating that more oxygen vacancies were constructed on the surface of Co-NW-R by H_2 reduction. Notably, loading Ag greatly increases the ratio of $O_{ads}/(O_{ads}+O_{lat})$ on the catalyst surface, as shown in Table 1, particularly for Ag/Co-NW-R. Additionally, the O 1 s peaks of the Ag-loaded catalysts shift to higher BEs, i.e., in the direction of the O_{ads} peaks. All of these results demonstrate that the enhanced metal–support interaction benefits the creation of surface-adsorbed oxygen species. It also coincides with the results of Co 2p XPS, soot-TPR, and CO-TPD.

Catalytic Soot Combustion Performance

Figure 6 and Table 2 display the soot-TPO activities and the corresponding CO_2 concentration profiles of the as-prepared monolithic catalysts in the absence or presence of 600-ppm NO. The blank experiment without any catalysts shows that T_{10}, T_{50}, and the CO_2 selectivity are 490 °C, 565 °C, and 55%, respectively. For all other samples, the only product of soot oxidation is CO_2, as listed in Table 2. Compared with the blank experiment, Ni foam can decrease the ignition temperature by 62 °C. Because of the excellent redox ability of Co_3O_4, Co-NW and Co-NW-R exhibit much higher catalytic soot oxidation activity than Ni foam alone. Evidently, after loading Ag NPs on them, T_{50} decreases remarkably, which indicates that Ag loading greatly promotes soot oxidation. The activities of the catalysts follow the order of Ag/Co-NW-R > Ag/Co-NW > Co-NW-R > Co-NW > Ni foam > Blank with and without NO. Introducing 600-ppm NO significantly lowers T_{10} and T_{50} for all as-prepared

catalysts but particularly for Ag/Co-NW-R. Notably, Co-NW-R exhibits only slightly higher catalytic activity than Co-NW, but the activity of Ag/Co-NW-R is much higher than that of Ag/Co-NW with and without NO. This result can be attributed to the enhanced metal–support interaction, high dispersion of Ag, and presence of more active oxygen species on Ag/Co-NW-R.

As a more effective oxidant than O_2, NO_2 can remarkably lower the oxidation temperature of soot particulates and plays a crucial role in the soot combustion process [43]. Thus, the ability to oxidize NO to NO_2 is a key factor influencing soot oxidation. Figure 7 shows the NO-TPO profiles of the catalysts. Apparently, loading Ag significantly lowers the NO oxidation temperatures and produces more NO_2 than the support alone, particularly for Ag/Co-NW-R.

Kinetic Study

To further understand the intrinsic activity of the catalysts, the isothermal anaerobic titration processes were carried out at 280 °C. Figure 8 shows the CO_2 concentration as a function of time before and after removing O_2 from the reactant flow. Table 3 and Fig. 8 display the corresponding kinetic results for the reaction rate, amount of O*, and TOF. Obviously, these values follow the order of Ag/Co-NW-R > Ag/Co-NW > Co-NW-R > Co-NW, which is consistent with the catalytic performance. Meanwhile, the parameters of Co-NW-R are only slightly larger than those of Co-NW, suggesting that the positive effect of the pre-reduced treatment of Co-NW on soot oxidation is limited. According to the Ag wt% measured by ICP, the reaction rate per gram of Ag on Ag/Co-NW-R is nearly 1.4-fold that on Ag/Co-NW, as shown in Table 3, demonstrating the higher utilization efficiency of Ag on Ag/Co-NW-R. Additionally, as shown in Table 3, compared with the supports, the Ag-loaded catalysts not only generate more active O* species but also achieve higher intrinsic activity (TOF), demonstrating the important effect of Ag-Co_3O_4 interactions on soot oxidation. Here compared with Ag/Co-NW, Ag/Co-NW-R has an only slightly higher TOF but an approximately 1.4-fold higher reaction rate. This result indicates that the primary function of the Ag-Co_3O_4 interaction is to improve the dispersion of Ag sites to increase the catalyst's apparent activity.
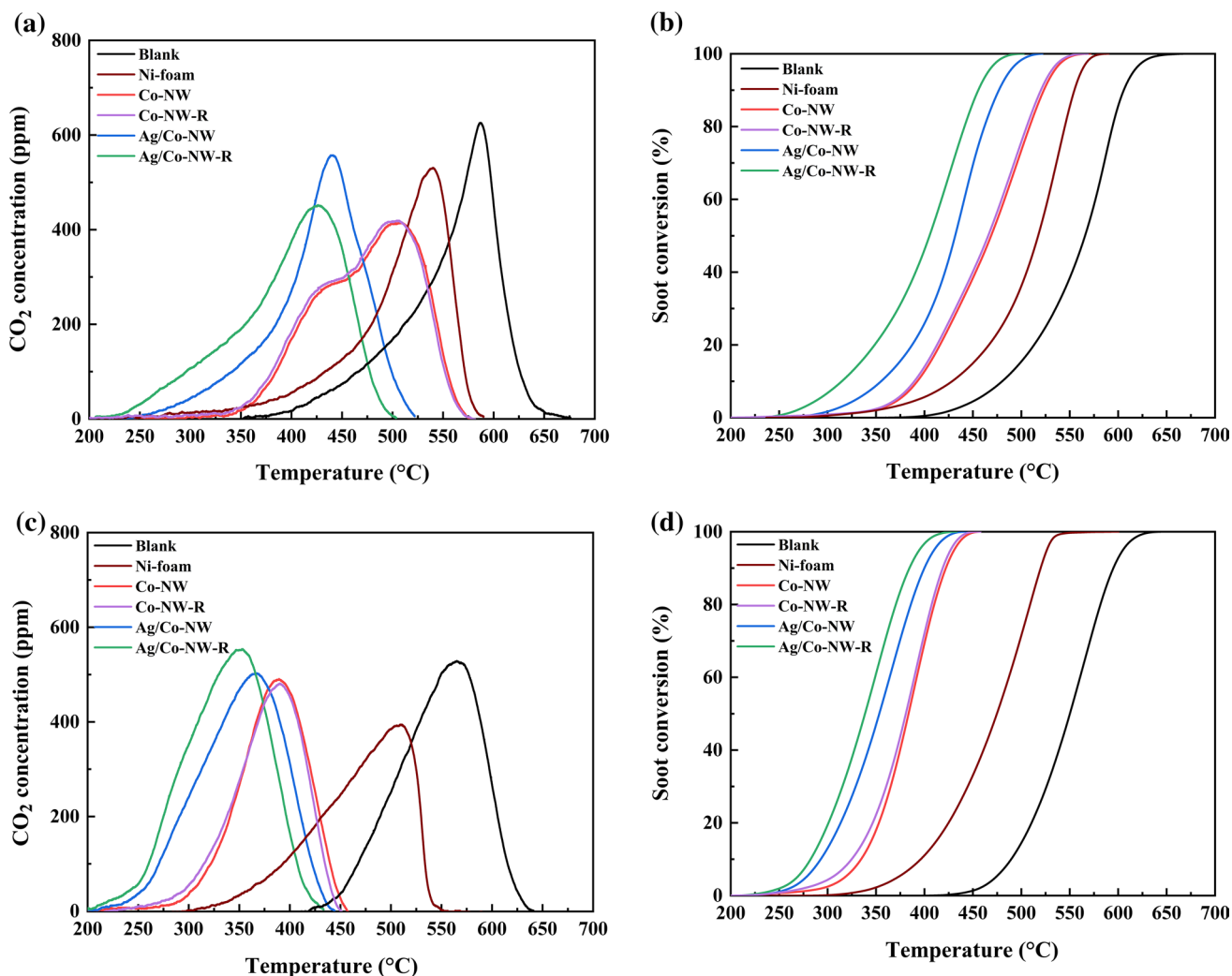
Fig. 6 **a**, **c** CO$_2$ concentration profiles and **b**, **d** soot conversion of the as-prepared catalysts during the soot-TPO reaction in **a**, **b** 10% O$_2$ balanced by N$_2$ and **c**, **d** 600-ppm NO and 10% O$_2$ balanced by N$_2$ under the loose contact condition

Table 2 Activities of the as-prepared catalysts in the presence or absence of 600-ppm NO for soot combustion

Catalysts	T_{10} (°C)		T_{50} (°C)		S_{CO2} (%)	
	0 ppm	600 ppm	0 ppm	600 ppm	0 ppm	600 ppm
Blank	490	480	565	550	55	60
Ni-foam	428	396	517	475	100	100
Co-NW	392	334	468	383	100	100
Co-NW-R	390	329	465	380	100	100
Ag/Co-NW	355	293	431	353	100	100
Ag/Co-NW-R	315	282	405	338	100	100

Catalytic Stability and Water Resistance

The catalytic stability and H$_2$O resistance of catalysts are crucial factors for soot combustion under practical conditions. Figure 9a displays five consecutive cycles of soot-TPO tests in NO/O$_2$/N$_2$ over Ag/Co-NW-R under loose contact

conditions. During the reaction, the catalyst and the soot were mixed in the same proportion to ensure as far as possible the same conditions for each test. T_{50} of Ag/Co-NW-R is very similar in each cycle, illustrating the high stability of this catalyst for soot oxidation. The soot-TPO experiment was performed over Ag/Co-NW-R in 10% H$_2$O/NO/O$_2$/N$_2$
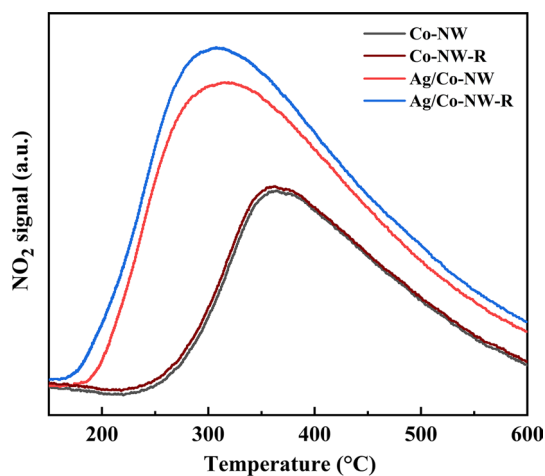
Fig. 7 Profiles of NO oxidation to NO_2 over the catalysts in a $NO/O_2/N_2$ atmosphere

to further investigate the impact of water vapor on soot combustion under the loose contact conditions. In Fig. 9b, introducing water vapor in the reactant flow improves the catalytic performance of Ag/Co-NW-R, which agrees with some previous reports [44, 45].

Discussion

Soot combustion is a redox reaction in nature. The active oxygen species play an important role in catalytic soot oxidation. In our work, the XPS results demonstrate that Ag species exist on the catalyst surface as Ag^0. For the catalytic soot oxidation in a N_2 atmosphere, as considered in Fig. 3, soot can only be oxidized by active oxygen species on the catalysts. In the range of 200–300 °C, little CO_2 is produced by oxidizing soot closely contacted with active sites. Compared with Co-NW, the CO_2 peak of the Ag-loaded catalysts
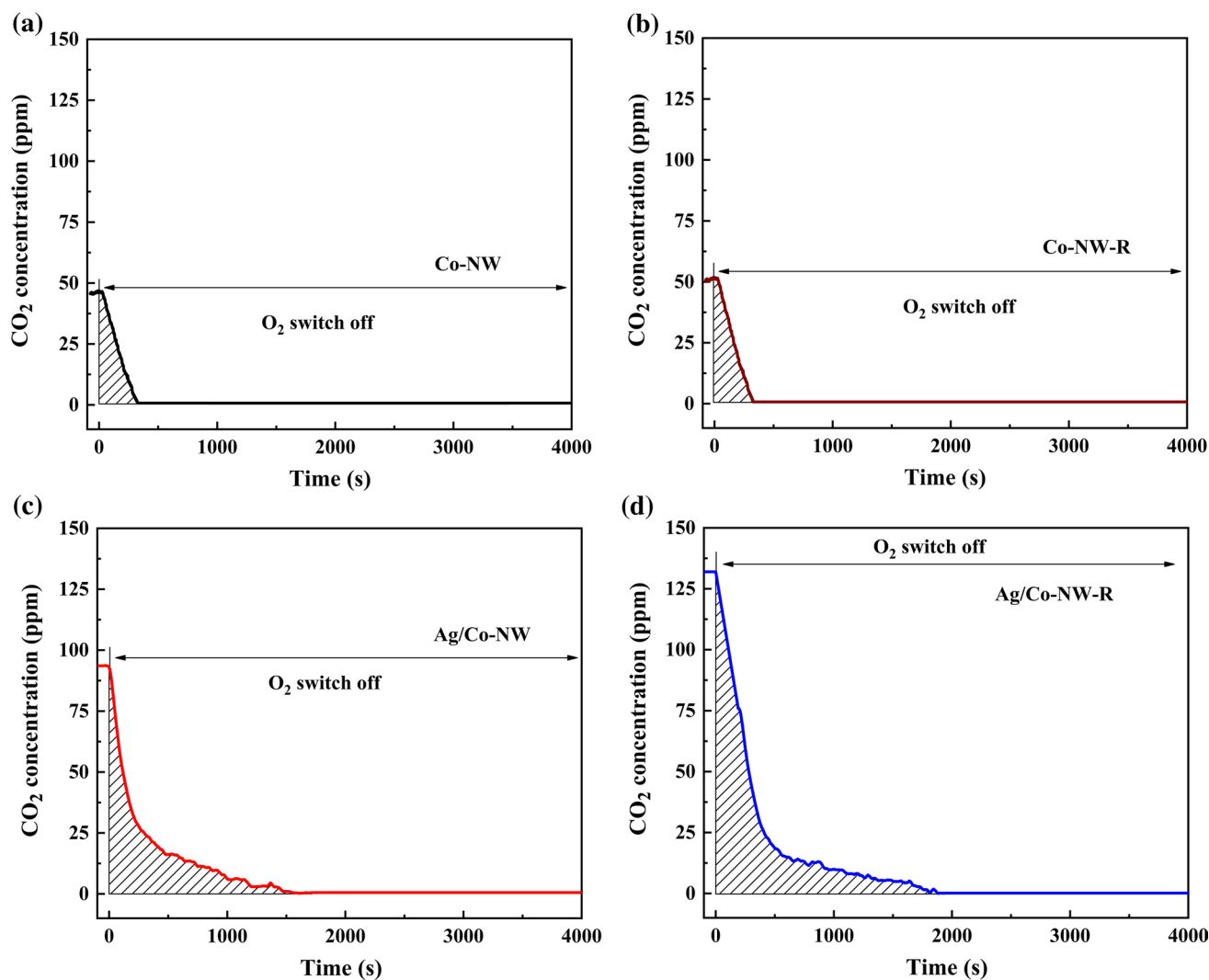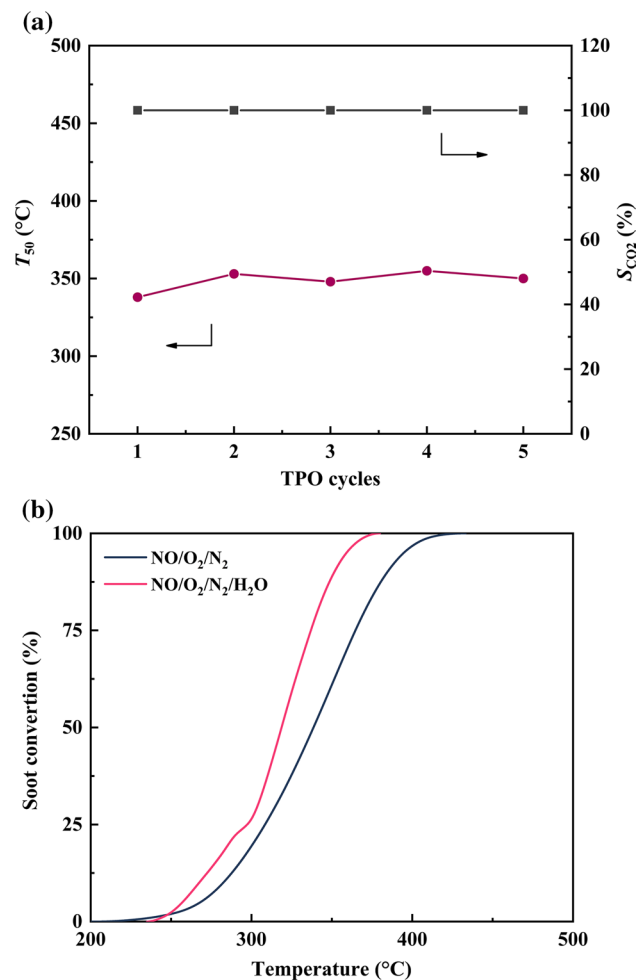

Fig. 8 Curves of CO_2 concentration as a function of time during isothermal soot oxidation at 280 °C under the loose contact conditions over the as-prepared catalysts **a** Co-NW, **b** Co-NW-R, **c** Ag/Co-NW, **d** Ag/Co-NW-R before and after O_2 is removed from the reactant flow

Table 3 Active oxygen (O*) amounts, reaction rates (ν, ν_{Ag}), and the TOF of the catalysts calculated from the results in Fig. 8

Catalysts	ν (10^{-7} mol/ (s·g$_{cat}$))	ν_{Ag} (10^{-6} mol/ (s·g$_{Ag}$))	O* amount (10^{-4} mol/g$_{cat}$)	TOF (10^{-3} s^{-1})
Co-NW	4.1	–	3.6	1.1
Co-NW-R	4.5	–	3.8	1.2
Ag/Co-NW	9.5	22.1	6.5	1.5
Ag/Co-NW-R	13.4	31.1	8.1	1.7

Fig. 9 **a** Stability of Ag/Co-NW-R in 600-ppm NO/10% O$_2$/N$_2$ and **b** water resistance of Ag/Co-NW-R in 600-ppm NO/10% O$_2$/N$_2$

shifts to lower temperatures, indicating that the oxidation ability of Ag sites is higher than that of Co-NW at low temperatures, particularly for Ag/Co-NW-R. With increasing temperature (400–600 °C), a large amount of soot is oxidized to CO$_2$ by surface lattice oxygen species, and the difference among the as-prepared catalysts is insignificant. However, when the temperature increases to 600 °C, soot is oxidized to

CO$_2$ by bulk lattice oxygen species of as-prepared catalysts. The Ag-loaded catalysts exhibit a larger CO$_2$ peak area due to the higher mobility of bulk lattice oxygen promoted by the Ag–Co$_3$O$_4$ interaction compared with their supports.

Conversely, after introducing gaseous oxygen, O$_2$ can be continuously activated and converted into reactive oxygen species at active sites. Compared with the reaction in the N$_2$ atmosphere, considered in Fig. 3, the soot oxidation performance of the catalysts improves substantially, and the shape of the CO$_2$ curves sharpens over the reaction temperature range (200–600 °C) in Fig. 6a, indicating a faster reaction rate in an O$_2$ atmosphere. Moreover, the CO$_2$ concentrations of the supports are quite low below 350 °C, while that of the Ag-loaded catalysts increases remarkably, demonstrating that the major function of Ag^0 sites is to activate gaseous oxygen molecules to oxidize soot. According to the results of soot-TPR, CO-TPD, O 1 s XPS, and TOF, Ag/Co-NW-R possesses the most surface oxygen species and the highest TOF value due to the enhanced metal–support interaction and thus shows the lowest ignition temperature and the highest apparent activity.

After being introduced to the reactant gas, NO is readily oxidized to NO$_2$, which is a better oxidant than O$_2$. Additionally, T_{10} and T_{50} of the as-prepared catalysts for catalytic soot oxidation continue to decrease in Fig. 6c, particularly for Ag/Co-NW-R. According to the NO-TPO results in Fig. 7, Ag/Co-NW-R shows the highest ability for oxidizing NO to NO$_2$ due to the promoted generation of active oxygen species by an enhanced metal–support interaction.

The above results indicate that the pre-reduction treatment on reducible supports effectively anchors metal sites, improves the metal dispersion, and enhances metal–support interactions, thereby increasing the number of active oxygen species and improving the intrinsic activity of catalysts for oxidation reactions.

Conclusions

In summary, in this work, we facilely synthesized Ag catalysts supported on Co$_3$O$_4$ nanowires in situ grown on monolithic Ni foam substrates. The designed catalyst exhibits high activity, stability, and water resistance for soot oxidation. Here, the Ag catalyst exists as Ag^0 due to the automatic reduction of Ag$^+$ by Co^{2+}. Interactions between Ag and Co$_3$O$_4$ improve the generation of active oxygen species to approximately twice that on the support alone. Through the reduction pretreatment of Co$_3$O$_4$ to generate more oxygen vacancies, Ag NPs with smaller sizes were highly dispersed and anchored thereon. In particular, this pretreatment not only increases the number of active oxygen species but also improves the intrinsic activity for soot oxidation. In addition, the macropores of the monolithic catalysts with crossed

Co$_3$O$_4$ nanowires can provide more soot–catalyst contact sites and increase the soot capturing efficiency. These advantages make the catalyst a possible candidate for industrial applications.

Supporting information

SEM images of the monolithic Ni foam (Fig. S1), the TEM-EDS mapping images of the Ag/Co-NW-R catalyst (Fig. S2), the corresponding size distribution of Ag NPs determined by HRTEM images (Fig. S3), and the average diameter (d_{Ag}) and dispersion (D_{Ag}) values of Ag NPs on monolithic catalysts (Table S1).

Declarations

References

1. Cao CM, Xing LL, Yang YX et al (2017) Diesel soot elimination over potassium-promoted Co$_3$O$_4$ nanowires monolithic catalysts under gravitation contact mode. Appl Catal B Environ 218:32–45
2. Gao ZN, Guo LH, Zhao DY, Xingang L et al (2021) Effect of a site-deficiency on the structure and catalytic oxidation activity of the La-Sr-Co-O perovskite. Chem J Chin Univ Chin 42:2869–2877
3. Yin MX, Liu DS, Li XG et al (2019) Effect of copper doping on lean NO$_x$ trap performance of Pt/Ba/Cu$_x$Mg$_{1-x}$Al$_2$O$_4$ catalysts at high temperatures. Chem J Chin Univ Chin 40:2170–2177
4. Zhang ZL, Zhang YX, Wang ZP et al (2010) Catalytic performance and mechanism of potassium-promoted Mg-Al hydrotalcite mixed oxides for soot combustion with O$_2$. J Catal 271(1):12–21
5. Yang YX, Zhao DY, Gao ZN et al (2021) Interface interaction induced oxygen activation of cactus-like Co$_3$O$_4$/OMS-2 nanorod catalysts in situ grown on monolithic cordierite for diesel soot combustion. Appl Catal B Environ 286:119932
6. Guan B, Lin H, Zhan R et al (2018) Catalytic combustion of soot over Cu, Mn substitution CeZrO$_{2-\delta}$ nanocomposites catalysts prepared by self-propagating high-temperature synthesis method. Chem Eng Sci 189:320–339
7. Ren W, Ding T, Li XG et al (2019) Identifying oxygen activation/oxidation sites for efficient soot combustion over silver catalysts interacted with nanoflower-like hydrotalcite-derived CoAlO metal oxides. ACS Catal 9(9):8772–8784
8. Aneggi E, Llorca J, de Leitenburg C et al (2009) Soot combustion over silver-supported catalysts. Appl Catal B Environ 91(1–2):489–498
9. Wu QQ, Xiong J, Zhang YL et al (2019) Interaction-induced self-assembly of Au@La$_2$O$_3$ core-shell nanoparticles on La$_2$O$_2$CO$_3$ nanorods with enhanced catalytic activity and stability for soot oxidation. ACS Catal 9(4):3700–3715
10. Fang F, Feng NJ, Wang L et al (2018) Fabrication of perovskite-type macro/mesoporous La$_{1-x}$K$_x$FeO$_{3-\delta}$ nanotubes as an efficient catalyst for soot combustion. Appl Catal B Environ 236:184–194
11. Xu JF, Liu J, Zhao Z et al (2010) Three-dimensionally ordered macroporous LaCo$_x$Fe$_{1-x}$O$_3$ perovskite-type complex oxide catalysts for diesel soot combustion. Catal Today 153(3–4):136–142
12. Zhao MJ, Deng JL, Sun YQ et al (2019) Roles of surface-active oxygen species on 3DOM cobalt-based spinel catalysts M$_x$Co$_{3-x}$O$_4$ (M = Zn and Ni) for NO$_x$-assisted soot oxidation. ACS Catal 9(8):7548–7567
13. Hernández WY, Lopez-Gonzalez D, Ntais S et al (2018) Silver-modified manganite and ferrite perovskites for catalyzed gasoline particulate filters. Appl Catal B Environ 226:202–212
14. Li Q, Meng M, Tsubaki N et al (2009) Performance of K-promoted hydrotalcite-derived CoMgAlO catalysts used for soot combustion, NO$_x$ storage and simultaneous soot-NO$_x$ removal. Appl Catal B Environ 91(1–2):406–415
15. Dai FF, Zhang YX, Meng M et al (2014) Enhanced soot combustion over partially substituted hydrotalcite-derived mixed oxide catalysts CoMgAlLaO. J Mol Catal A Chem 393:68–74
16. Li Q, Wang X, Xin Y et al (2014) A unified intermediate and mechanism for soot combustion on potassium-supported oxides. Sci Rep 4:4725
17. Li Q, Wang X, Chen H et al (2016) K-supported catalysts for diesel soot combustion: making a balance between activity and stability. Catal Today 264:171–179
18. Shang Z, Sun M, Chang SM et al (2017) Activity and stability of Co$_3$O$_4$-based catalysts for soot oxidation: the enhanced effect of Bi$_2$O$_3$ on activation and transfer of oxygen. Appl Catal B Environ 209:33–44
19. Andana T, Piumetti M, Bensaid S et al (2016) Nanostructured ceria-praseodymia catalysts for diesel soot combustion. Appl Catal B Environ 197:125–137
20. Corro G, Vidal E, Cebada S et al (2017) Electronic state of silver in Ag/SiO$_2$ and Ag/ZnO catalysts and its effect on diesel particulate matter oxidation: an XPS study. Appl Catal B Environ 216:1–10
21. Li L, Yang QL, Zhang CY et al (2019) Hollow-structural Ag/Co$_3$O$_4$ nanocatalyst for CO oxidation: interfacial synergistic effect. ACS Appl Nano Mater 2(6):3480–3489
22. Chen LW, Li T, Zhang J et al (2021) Chemisorbed superoxide species enhanced the high catalytic performance of Ag/Co$_3$O$_4$ nanocubes for soot oxidation. ACS Appl Mater Interfaces 13(18):21436–21449
23. Lin J, Wang XD, Zhang T (2016) Recent progress in CO oxidation over Pt-group-metal catalysts at low temperatures. Chin J Catal 37(11):1805–1813

24. Liang HY, Jin BF, Li M et al (2021) Highly reactive and thermally stable Ag/YSZ catalysts with macroporous fiber-like morphology for soot combustion. Appl Catal B Environ 294:120271

25. Liu S, Wu XD, Liu W et al (2016) Soot oxidation over CeO$_2$ and Ag/CeO$_2$: factors determining the catalyst activity and stability during reaction. J Catal 337:188–198

26. Lee JH, Jo DY, Choung JW et al (2021) Roles of noble metals (M = Ag, Au, Pd, Pt and Rh) on CeO$_2$ in enhancing activity toward soot oxidation: active oxygen species and DFT calculations. J Hazard Mater 403:124085

27. Grabchenko MV, Mamontov GV, Zaikovskii VI et al (2020) The role of metal-support interaction in Ag/CeO$_2$ catalysts for CO and soot oxidation. Appl Catal B Environ 260:118148

28. Wang X, Jin BF, Feng RX et al (2019) A robust core-shell silver soot oxidation catalyst driven by Co$_3$O$_4$: effect of tandem oxygen delivery and Co$_3$O$_4$-CeO$_2$ synergy. Appl Catal B Environ 250:132–142

29. Cheng Y, Liu J, Zhao Z et al (2017) Highly efficient and simultaneously catalytic removal of PM and NOx from diesel engines with 3DOM Ce0.8M0.1Zr0.1O2 (M = Mn Co, Ni) catalysts. Chem Eng Sci 167:219–228

30. Yu XH, Ren Y, Yu D et al (2021) Hierarchical porous K-OMS-2/3DOM-m Ti0.7Si0.3O2 catalysts for soot combustion: easy preparation, high catalytic activity, and good resistance to H2O and SO2. ACS Catal 11(9):5554–5571

31. Xiong J, Wei YC, Zhang YL et al (2020) Synergetic effect of K sites and Pt nanoclusters in an ordered hierarchical porous Pt-KMnOx/Ce0.25Zr0.75O2 catalyst for boosting soot oxidation. ACS Catal 10(13):7123–7135

32. Shi QL, Liu TZ, Li Q et al (2019) Multiple strategies to decrease ignition temperature for soot combustion on ultrathin MnO$_{2-x}$ nanosheet array. Appl Catal B Environ 246:312–321

33. Mei XY, Zhu XB, Zhang YX et al (2021) Decreasing the catalytic ignition temperature of diesel soot using electrified conductive oxide catalysts. Nat Catal 4(12):1002–1011

34. Xing LL, Yang YX, Li XG et al (2018) Decorating CeO$_2$ nanoparticles on Mn$_2$O$_3$ nanosheets to improve catalytic soot combustion. ACS Sustain Chem Eng 6(12):16544–16554

35. Zhang L, Zhang CB, He H (2009) The role of silver species on Ag/Al$_2$O$_3$ catalysts for the selective catalytic oxidation of ammonia to nitrogen. J Catal 261(1):101–109

36. Zhang ZL, Han D, Wei SJ et al (2010) Determination of active site densities and mechanisms for soot combustion with O$_2$ on Fe-doped CeO$_2$ mixed oxides. J Catal 276(1):16–23

37. Liu ZQ, Li JH, Buettner M et al (2019) Metal-support interactions in CeO$_2$- and SiO$_2$-supported cobalt catalysts: effect of support morphology, reducibility, and interfacial configuration. ACS Appl Mater Interfaces 11(18):17035–17049

38. Duan D, Hao CX, He GG et al (2020) Co$_3$O$_4$ nanosheet/Au nanoparticle/CeO$_2$ nanorod composites as catalysts for CO oxidation at room temperature. ACS Appl Nano Mater 3(12):12416–12426

39. Yu L, Peng RS, Chen LM et al (2018) Ag supported on CeO$_2$ with different morphologies for the catalytic oxidation of HCHO. Chem Eng J 334:2480–2487

40. Ma XY, Yu XL, Ge MF (2021) Highly efficient catalytic oxidation of benzene over Ag assisted Co$_3$O$_4$ catalysts. Catal Today 376:262–268

41. Liu BC, Liu Y, Li CY et al (2012) Three-dimensionally ordered macroporous Au/CeO$_2$-Co$_3$O$_4$ catalysts with nanoporous walls for enhanced catalytic oxidation of formaldehyde. Appl Catal B Environ 127:47–58

42. Bai BY, Li JH (2014) Positive effects of K$^+$ ions on three-dimensional mesoporous Ag/Co$_3$O$_4$ catalyst for HCHO oxidation. ACS Catal 4(8):2753–2762

43. Cao CM, Xing LL, Yang YX et al (2017) The monolithic transition metal oxide crossed nanosheets used for diesel soot combustion under gravitational contact mode. Appl Surf Sci 406:245–253

44. Zhou XX, Chen HR, Zhang GB et al (2015) Cu/Mn co-loaded hierarchically porous zeolite beta: a highly efficient synergetic catalyst for soot oxidation. J Mater Chem A 3(18):9745–9753

45. Ranji-Burachaloo H, Masoomi-Godarzi S, Khodadadi AA et al (2016) Synergetic effects of plasma and metal oxide catalysts on diesel soot oxidation. Appl Catal B Environ 182:74–84

Chunmei Cao received her B.E. (2012) and PhD degrees (2017) in Chemical Engineering from Zhengzhou University and Tianjin University, respectively. She joined School of Chemical Engineering at Zhengzhou University in 2017 as Lecturer. Her current research interests focus on the development of nanomaterials for catalytic oxidation, including catalytic soot/VOCs oxidation and selective catalytic oxidation of cyclohexane.

Xingang Li is the Dean of Department of Catalysis Science & Engineering and Chair Professor in Tianjin University. He achieved his BS (1998) and PhD degree (2003) from University of Science & Technology of China. After finishing the postdoctoral research at IRCELyon (France) and University of Patras (Greece), in 2007 he joined School of Chemical Engineering & Technology of Tianjin University as Associate Professor. In 2013 and 2018, he was promoted as Full Professor and Tenure checked Professor, respectively. He published more than 150 articles and patents, served as the Associate Editor of "Journal of Chemical Technology & Biotechnology", and Guest Editor of "Catalysis Today" and "CIESC Journal", and was awarded the "Young Scientist Award" by the International Association of the Catalysis Societies (IACS). His research interests include C1 chemistry, hydrogen energy catalysis, and environmental catalysis.